

TWO DIMENSIONAL DYNAMIC STALL

Horia Dumitrescu*, Alexandru Dumitrache*¹

*Institute of Mathematical Statistics and Applied Mathematics,
Str. Calea 13 Septembrie, No.13, Sector 5, Bucharest, ROMANIA
horiad@ima.ro

ABSTRACT

Flow fields generated by aircraft manoeuvres and departure at high angles of attack are highly complex due to the simultaneous presence and interaction of three-dimensionality, unsteadiness, separation and reattachment influences. In order to come to grips with, the modeling of such a formidable flow regime it is necessary to start with a simpler flow regime in which flow separation and reattachment play a fundamental role. Two-dimensional dynamic stall fits the bill and so it has been investigated.

Therefore an axiomatic aerodynamic model has been developed for the general motion of a two dimensional airfoil as it passes in and out of stall, which gives realistic unsteady loads as compared to experimental values.

1. INTRODUCTION

The phenomenon of dynamic stall on oscillating two-dimensional airfoils has been studied for many years, both as an important practical problem in the context of helicopter rotors and as a challenging fundamental problem in its own right.

Dynamic stall can be divided into a number of distinct stages [1, 2]. Figure 1 shows the typical dynamics hysteresis in C_L and C_M and with angle $\theta(t)$ as $\theta(t)$ oscillates about a mean value of 15° with an amplitude of 10° at a non-dimensional frequency $k(= \omega c / V)$ equal to 0.20 (in aircraft dynamic notation the incidence angle $\alpha(t)$ is equal to $\theta(t)$, so the airfoil has both a pitch rate $\dot{\theta}(t)$ and incidence rate $\dot{\alpha}(t)$). The static curves for C_L and C_M against θ are shown in Fig. 1 as dotted curves; the static curve in this case has no hysteresis although for other airfoils a small static hysteresis behaviour can occur. In the dynamic case the flow remains attached to a higher angle of θ than that for steady stall, ($\theta = \theta_1$ in Fig. 1) Sometime after θ exceeds the static stall angle (i.e. $\theta > \theta_1$), a thin layers of reversed flow develops on the upper surface.

¹ *Institute of Mathematical Statistics and Applied Mathematics,
Str. Calea 13 Septembrie, No.13, Sector 5, Bucharest, ROMANIA
E-mail:horiad@ima.ro

Flow separation occurs later (when $\theta = \theta_3$ in Fig. 1), the separation may take form of a trailing edge separation which starts towards the rear of the airfoil and moves quickly forward to the leading edge or as a sudden leading edge separation. In either case, a vortex forms near the leading edge region and then convects rearward at a speed about half of the free stream velocity. The lift continues to increase until the vortex is well past mid-chord. The associated change in the pressure distribution causes the $\frac{1}{4}$ -chord pitching moment to plunge to a large negative value. As the vortex nears the trailing edge, the lift and moment reach peaks, although usually not simultaneously and then change dramatically.

As θ decreases to an angle about that for steady reattachment, a reattachment point forms near the/nose and moves rearward at a speed below the free stream velocity. When the reattachment reaches the trailing edge the flow is fully attached, by this time the angle θ is well below the steady reattachment angle.

The objective of this paper is to build an axiomatic theoretical model which duplicates the various stages of dynamic stall on an airfoil, and then investigate the implications of the axiomatic model in dynamic response.

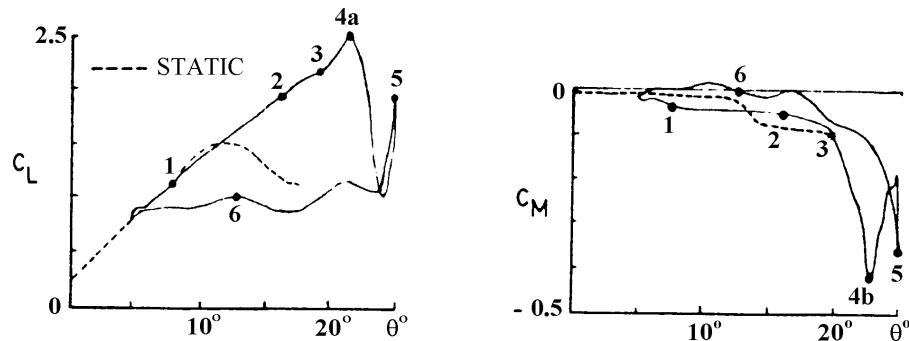


Fig.1 – Dynamic stall events on the VERTOL VR-7 aerofoil at $M_\infty = 0.25$,
 $\theta = 15^\circ + 10^\circ \sin \omega t$,
and $v = 0.10$ points defined in Table 1.

Table 1

Point	Flow Structure	Forces and Moments
1	Thin attached boundary layer	Linear regime
2	Flow reversal within boundary layer	Exceed static $C_{L \max}$ extrapolate linear regime
3	Vortex detaches and moves over airfoil surface	Pitching moment diverges, vortex lift present
4	Vortex continues towards trailing edge	Maximum lift and moment, followed by rapid decay
5	Secondary vortex	Secondary peaks
6	Reattachment of flow from leading edge	Readjust to linear regime

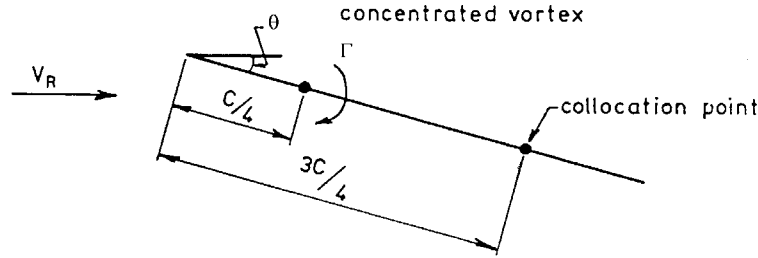


Fig. 2 – Model for steady attached flow

2. AXIOMATIC MODEL

2.1. Steady state, below stall (no separation)

For an airfoil at a steady angle of attack below the static stall angle the axiomatic model, as shown in Fig. 2, consists of a concentrated vortex placed on the $\frac{1}{4}$ -chord line and the boundary condition of tangency of flow is satisfied on the $\frac{3}{4}$ -chord line. This model is known to give the correct steady value of C_L and C_M for a symmetric airfoil throughout the angle of attack range for attached flow.

2.2 Steady state, above stall (leading edge separation)

For an airfoil at a steady angle of attack above the static stall angle (taken to be 12°) the axiomatic model, shown in Fig. 3 consists of the following features.

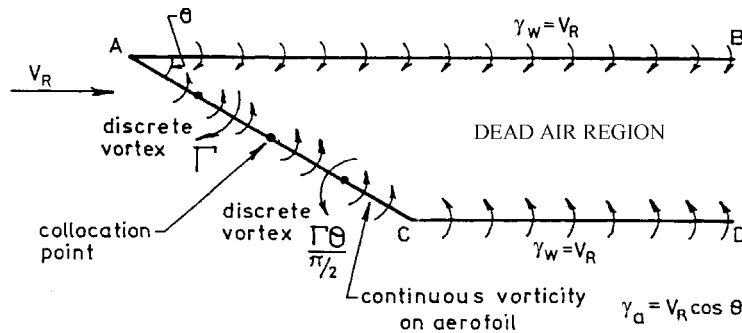


Fig. 3 – Model for steady flow.

1) separating streamlines of continuous vorticity extend from both the airfoil leading edge and airfoil trailing to infinity enclosing a dead air region the strengths of these convected vortex sheets γ_w are taken to be $\pm V_R$ as indicated in Fig. 3, namely difference in velocity between the free stream velocity and dead air region;

2) assuming a dead air region aft of the airfoil, a uniform vorticity distribution γ_a is introduced on the airfoil chord of strength $V_R \cos \theta$ in order to cancel out locally the freestream velocity behind the airfoil in the wake;

3) a discrete bound vortex of strength Γ is placed on the $\frac{1}{4}$ -chord line;

4) a discrete bound vortex of strength $(-\Gamma 2\theta / \pi)$ is placed on the $\frac{3}{4}$ -chord line on the argument that for small angle θ the vortex strength on the $\frac{3}{4}$ -chord line is small but as $\theta \rightarrow \pi/2$ the vorticity must be antisymmetric about the airfoil mid-chord;

5) since there is only one unknown Γ to be determined at a particular angle θ only one collocation point is required; this collocation point, where the condition of tangency of flow is to be satisfied, is taken at the mid-chord point, chosen to ensure symmetry about the mid-chord as $\theta \rightarrow \pi/2$.

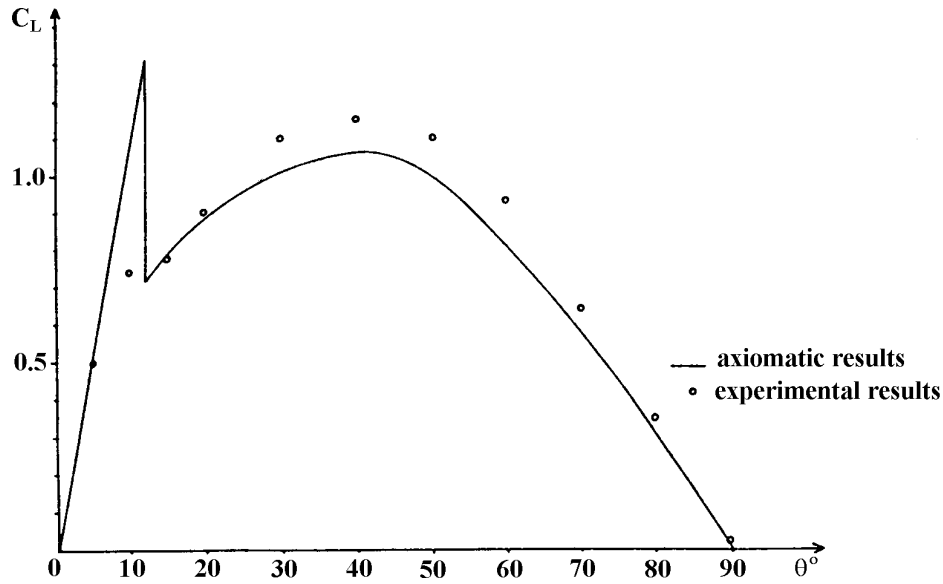


Fig. 4 – Graph of steady C_L versus incidence θ .

Once Γ has been calculated then the normal force on airfoil can be determined from the forces on the two discrete vortices ($\Gamma, -\Gamma 2\theta / \pi$), from the resultant normal force on the airfoil vorticity γ_a , and with a further contribution from an empirical uniform loading ΔH , which allows for the difference in total head across the airfoil. For predicted results to compare with experimental data the variation of the ΔH term with angle θ takes the form of a linear variation from $1.6\left(\frac{1}{2}\rho V_R^2\right)$ when θ is 12° , the stall angle, up to $2.0\left(\frac{1}{2}\rho V_R^2\right)$ when θ is 45° , for θ above 45° $\left(\Delta H / \frac{1}{2}\rho V_R^2\right)$ is taken to be constant and equal to 2.0, a reasonable value of C_N compared with experiment for a tow-dimensional plate normal to a free stream.

The comparison of the axiomatic lift coefficient with a typical set of experimental data [4] is shown in Fig. 4, where the sudden drop in C_L at the stall is not untypical for a leading edge stall. Figure 5 shows C_{M0} , the moment coefficient about the leading edge, derived from the axiomatic model. It is of interest to note that the discontinuity in C_{M0} at stall is small due to the fact that when the airfoil stalls the loss in lift is compensated by an aft movement of the centre of pressure. The discontinuity in the rate of change of C_{M0} at θ equal to 45° is due to the change in the variation of ΔH with θ .

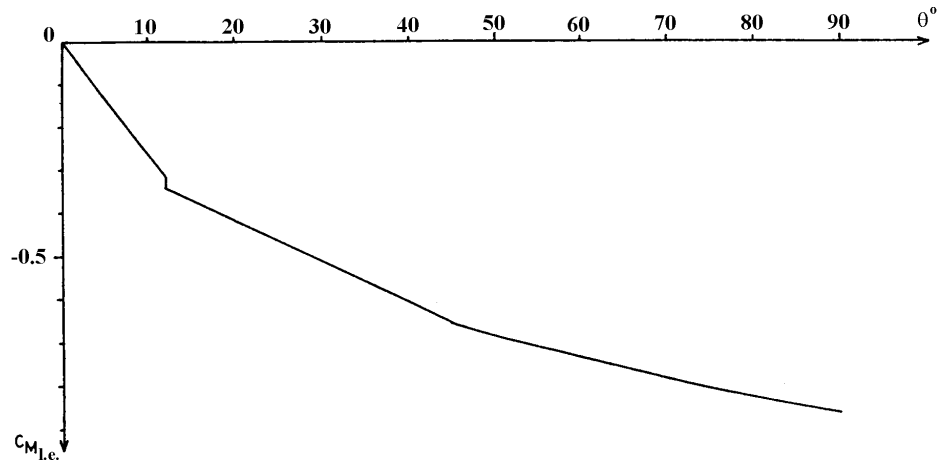


Fig. 5 - Graph of steady $C_{M_{l.e}}$ versus incidence

2.3 Unsteady motion below stall (trailing edge separation)

Suppose that the airfoil is pitching about its leading edge, defining the time dependent pitch angle $\theta(t)$ as shown in Fig. 6. Suppose that for $t < t_0$ the airfoil is steady at the inclined angle $\theta = \theta_0$ so that a steady circulation Γ_0 acts about the airfoil. With the model already formulated Γ_0 is assumed to be concentrated into a line vortex located on the $\frac{1}{4}$ -chord line.

If the time-dependent motion starts at t_0 , then after a time interval $\Delta t (= c / V_R$, the time taken for the free stream to travel one chord) the pitch angle will be θ_1 and the model of vorticity is a discrete vortex of strength Γ_1 located on the $\frac{1}{4}$ -chord line with a shed vortex, of strength $(-\Gamma_1 + \Gamma_0)$ located on the line one chord aft of Γ_1 , that is on the line $\frac{1}{4}$ -chord aft of trailing edge as shown in Fig. 6. The overall circulation remains constant in accordance with Kelvin's theorem. The value of Γ_1 is found from the boundary condition that the normal induced velocity due to Γ_1 and Γ_0 , at the $\frac{3}{4}$ -chord collocation point, together with the normal component of the free stream velocity, is equal to the normal velocity of the airfoil section at that collocation point.

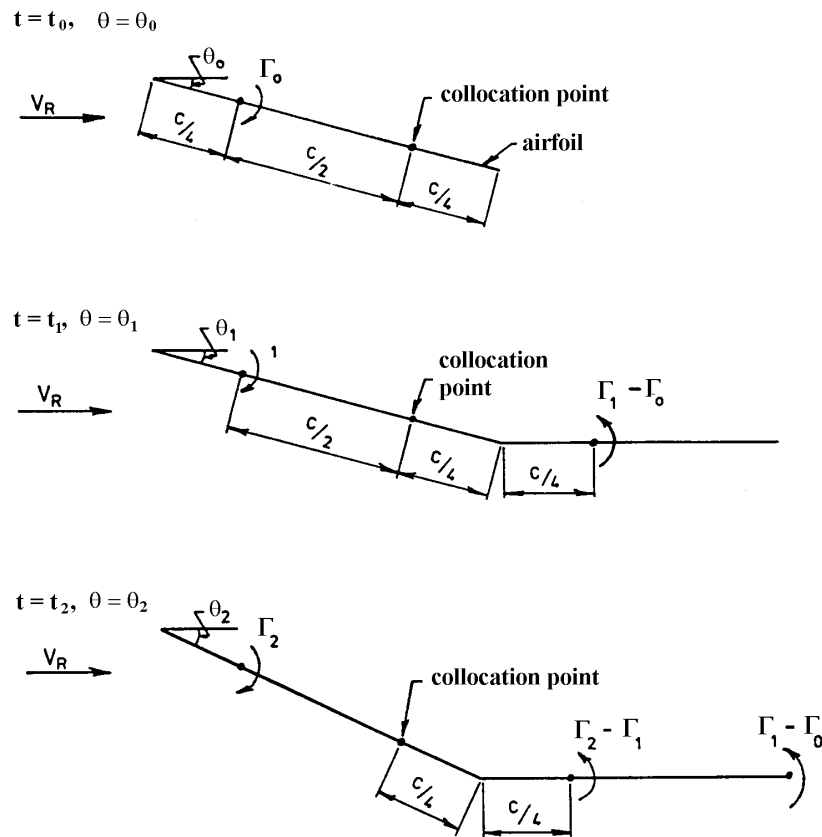


Fig. 6 - Attached flow past an unsteady airfoil

After the next time interval (i.e., at time $t_2 = t_1 + \Delta t$) when θ is equal to θ_2 , the pattern of vortices, as shown in Fig. 6, comprises.

- 1) a bound vortex of strength Γ_2 on the $1/4$ -chord line;
- 2) a newly shed vortex of strength $(-\Gamma_2 + \Gamma_1)$ on the $1/4$ -chord line aft of the trailing edge;
- 3) the convected vortex of strength $(-\Gamma_1 + \Gamma_0)$ now located on the $5/4$ -chord line aft of the trailing edge.

The strength of the vortex Γ_2 is given by applying the condition of tangency of flow at the $3/4$ -chord point in the same way as at time t_1 , as explained above. This sequence can be continued in time intervals of Δt .

This model is reasonable for slow rates of change such as overall aircraft motions in a stability and control context because of the relatively long aerodynamic time interval of $\Delta t (= c / V_R)$, which it is rather too long for aeroelastic phenomena such as flutter.

The above, axiomatic model of unsteady attached flows has been applied to an airfoil oscillating in pitch about an axis at the leading edge in a steady flow of velocity V_R with $\theta(t)$ equal to $\theta_0 \sin \omega t$. Values taken are $\theta_0 = 10^\circ$, $c = 1$ m and $V_R = 30$ m/s. $C_L(t)$ at different rates of oscillations are found and compared with the quasi-steady formula ($C_L = 2\pi\theta(t)$).

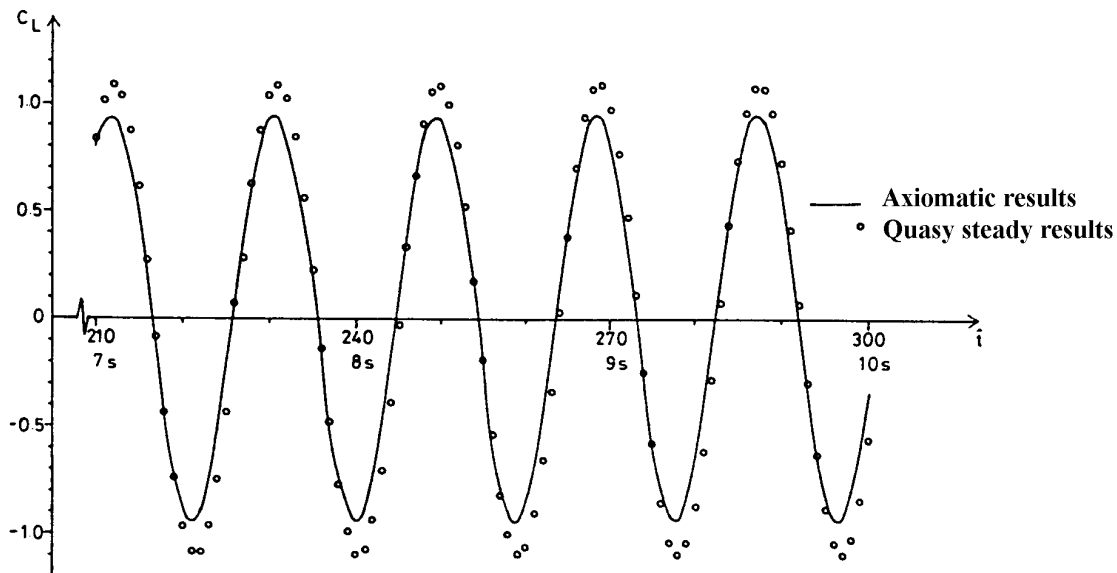


Fig. 7 - Aerofoil oscillating in a steady flow, $v = \omega c/V_R = 0.333$.

Results for C_L are shown in Fig. 7 when $v (= \omega c/V)$ the frequency parameter is equal to $1/3$. The difference between the oscillatory and quasi-steady results is noted the oscillatory amplitude is approximately 14% less than the quasi-steady value (the value from unsteady linearised theory is about 16%). A slight phase difference exists between the input θ and C_L (the theoretical value is also small).

2.4. Development of unsteady separation (leading edge separation)

Next it is necessary to formulate an axiomatic process of separation as the time-varying airfoil angle passes up through the static angle of 12° and continues to increase. Consider the case where $\theta(t)$ is increasingly monotonically from a low value to a higher value.

It is known from experiments that there is a delay in the onset separation for a dynamic approach to stall. It is assumed that onset of separation is delayed by one time step (i.e. for a delay time Δt); this time delay is not arbitrary, it fits closely with experimental behaviour. Thus if θ_i (at $t = t_i$) is less than 12° and if θ_{i+1} (at $t = t_{i+1}$) is above 12° then it is assumed that attached flow continues until and including θ_{i+2} (at $t = t_{i+2}$). While the unsteady flow remains attached the unsteady vortex model is that described previously. This model is reproduced in Figs. 8(I), 8(II), which shows the vortex pattern at time t_i, t_{i+1}, t_{i+2} , for $\theta_i, \theta_{i+1}, \theta_{i+2}$.

A separation pattern model for $\theta > \theta_{i+2}$, at $t > t_{i+2}$ develops progressively. At times t_{i+3} , and t_{i+4} it is assumed that separation occurs at the leading edge and it takes increment of time $2\Delta t$ for the leading edge vorticity to form. This stage is called half or incipient separation and it is shown in Fig. 8(III). Continuous vorticity of strength V_R is placed on the developing upper separation streamline together with an associated vorticity of strength $V_R \cos \theta$ over the foremost half-chord of the airfoil. There is the one discrete vortex Γ_{i+4} on the airfoil $1/4$ -chord line, and the shed vorticity associated with the change in strength of the airfoil discrete vortices is convected aft of the trailing edge. The collocation point to determine Γ_{i+4} remains at the $3/4$ -chord point. It is assumed that the continuous vorticities do not contribute to the downwash at the collocation point so Γ_{i+4} is calculated according to the same formulae as in attached conditions. But half

separation is characterized however by an increase in normal force.

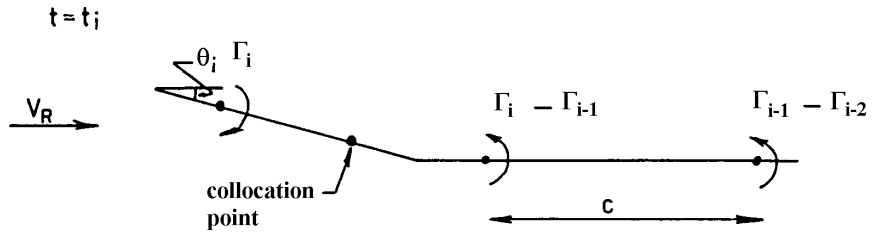
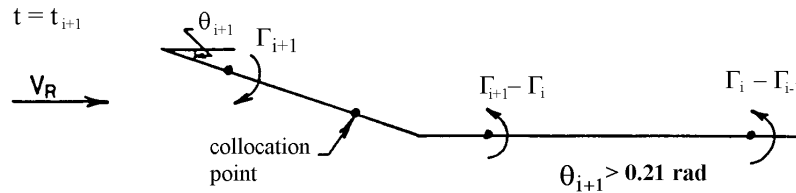


Fig. 8(i) Attached flow, $\theta_i < 0.21 \text{ rad } (12^\circ)$.



Similar pattern
at t_{i+2}

Fig. 8 (ii) Separation delay .

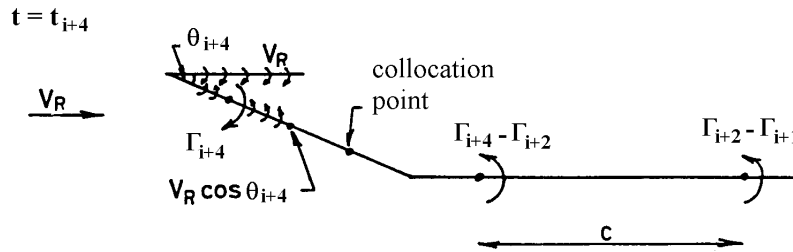


Fig. 8 (iii) Half separation ($\theta_{i+4} > \theta_{i+2}$).

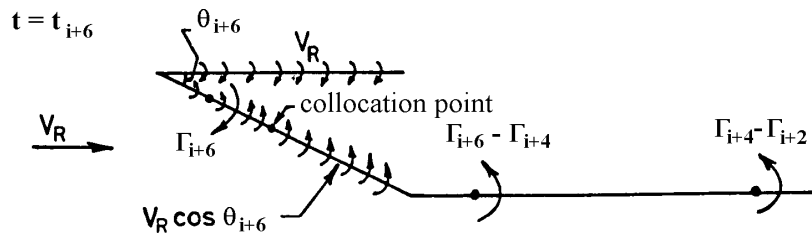


Fig. 8 (iv) Separation ($\theta_{i+6} > \theta_{i+4}$).

After half separation it is assumed that it takes two further increment of $\Delta t(t_{i+6})$ for the leading edge separation to extend to 1 chord aft of the leading edge.

As shown in Fig. 8(IV) the upper streamline vorticity of strength V_R now extends about 1 chord aft of the leading edge with vorticity of strength $V_R \cos \theta_{i+6}$ on the airfoil

chord. There is still one discrete vortex Γ_{i+6} on the $\frac{1}{4}$ -chord line. The collocation point is now switched on the $\frac{1}{2}$ -chord point. This flow regime is called separation. At separation the empirical difference factor ΔH needs to be introduced. The empirical value of $(\Delta H / 1/2\rho V_R^2)$ is taken to be 2.0, which is higher than in the steady separation model at low angles but it appears necessary to do so in order to obtain reasonable results.

For $t > t_{i+8}$ separating streamlines of uniform vorticity $(\pm V_R)$ extend from both the airfoil leading edge and airfoil trailing edge to infinity enclosing a dead air region. There is also a uniform vorticity distribution $V_R \cos \theta$ on the airfoil chord and two discrete bound vortices of strength Γ and $(-\Gamma 2\theta / \pi)$ are placed on the $\frac{1}{4}$ and $\frac{3}{4}$ -chord line respectively. A major assumption is that the whole time varying shed vorticity is placed in discrete vortices shed from the trailing edge, that appear to be reasonable when the airfoil pitch angle is increasing.

The shed vortices from the trailing edge are assumed to convect downstream with velocity $.V_R / 2$ (i.e. at half the speed in the attached flow regime) on the argument that the mean velocity of convection between the dead air enclosed within the wake and the freestream is $V_R / 2$. Subsequent calculations are carried out in time increments of $2\Delta t$. The patterns at full separation at times t_{i+8} and t_{i+10} are shown in Fig. 8(V, VI).

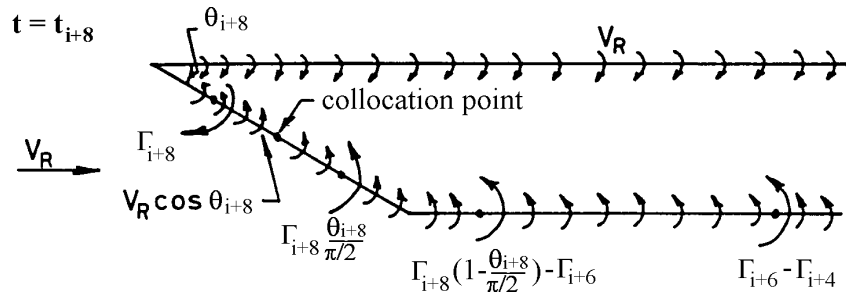


Fig. 8 (v) Full Separation $(\theta_{i+8} > \theta_{i+6})$.

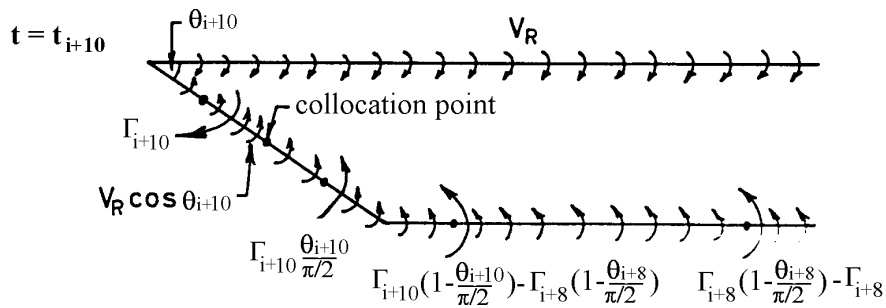


Fig. 8 (vi) Full Separation $(\theta_{i+10} > \theta_{i+8})$.

To validate the model numerical results for the normal force on an airfoil, when the angle of attack is increasing at a uniform rate, are compared with experiment and are shown in Fig. 9. The experimental results are taken from Ref. 3. In the experiments a two-dimensional airfoil model having a NACA 0012 profile with a 0.2 m chord is mounted on a pitch rig in a wind tunnel. The airfoil is then subjected to an increase of angle of attack with angular velocities 5.74 rad/s in a freestream velocity of 19.2 m/s. The results are measured by two different methods: by means of strain gauges and pressure transducers. For both cases the numerical model gives more normal force in the initial

half separation stage. Numerical $C_{N \max}$ agrees closely with experimental $C_{N \max}$. Therefore, the axiomatic model gives acceptable trends for a motion with increasing incidence.

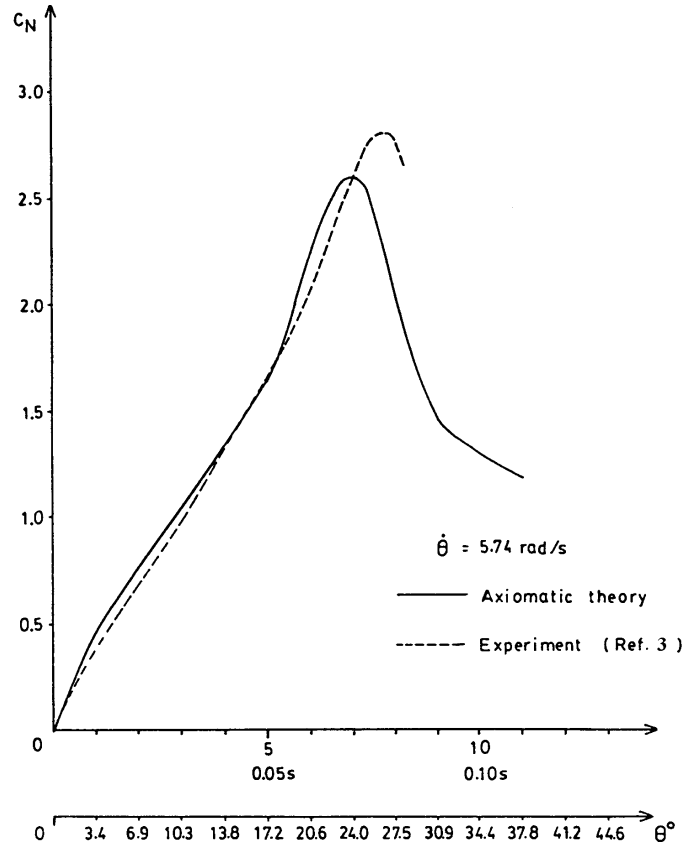


Fig. 9 – Constant rate of increase of pitch angle.

2.5. Development of unsteady reattachment

The process of unsteady flow reattachment is now modeled. Suppose for $t < t_i$, the flow is steady in a separated state (Fig. 10(I)), and then θ decreases with time. At t_{i+2} , $\theta_{i+2} < \theta_i$ assuming that θ_{i+2} is greater than $0.21 \text{ rad} (=12^\circ)$, the model is virtually the same as at time t_i except that the shed discrete vortex is now shed along the top dividing streamline (Fig. 10(II)).

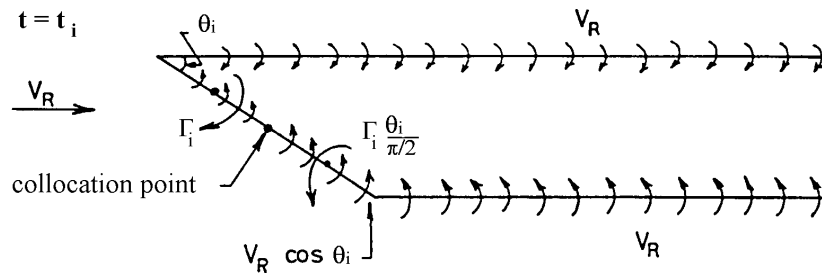


Fig 10 (i) – Steady separated flow $\theta_i > 0.21 \text{ rad} (12^\circ)$.

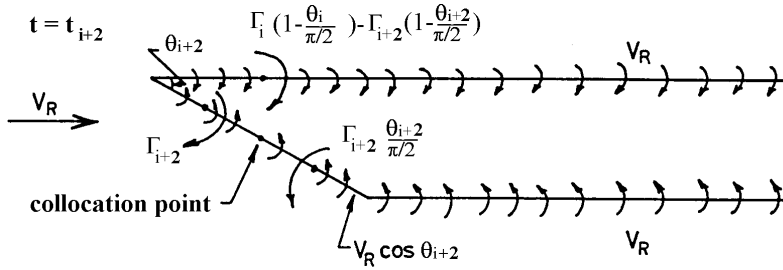


Fig. 10 (ii) - Unsteady separated flow, $\theta_i > \theta_{i+2} > 0.21 \text{ rad}$.

If θ_{i+4} is still greater than 0.21 rad then the same model applies as shown in Fig. 10(III). At t_{i+6} when the pitch angle θ_{i+6} is less than 0.21 rad it is assumed that the flow begins to reattach. As shown in Fig. 10(IV), the upper dividing separation streamline now moves down the airfoil surface and starts from the airfoil $\frac{1}{2}$ -chord line. The continuous vorticity on the airfoil also moves down to the aft airfoil behind $\frac{1}{2}$ chord line. A single discrete vortex is located on the $\frac{1}{4}$ -chord line. The collocation point is switched to the $\frac{3}{4}$ -chord line. This stage of flow reattachment is called incipient or half reattachment.

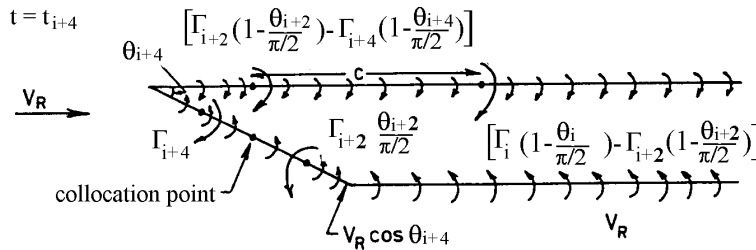


Fig. 10 (iii) - Unsteady separated flow, $\theta_{i+2} > \theta_{i+4} > 0.21 \text{ rad}$.

With a further single increment of time at t_{i+7} , the flow becomes fully attached as shown in Fig. 10(V) where a discrete vortex at the airfoil $\frac{1}{4}$ -chord and discrete vortices in the planar wake are the only form of vorticity left in the system. No experimental results with decreasing θ are available. It is noted that the flow separation takes a much longer time to build up than for flow reattachment to establish itself, this behaviour being a strong feature of real flows.

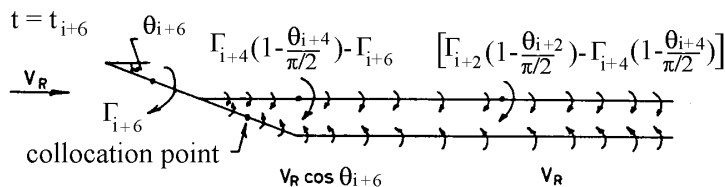


Fig. 10 (iv) - Unsteady reattachment, $\theta_{i+6} < 0.21 \text{ rad}$.

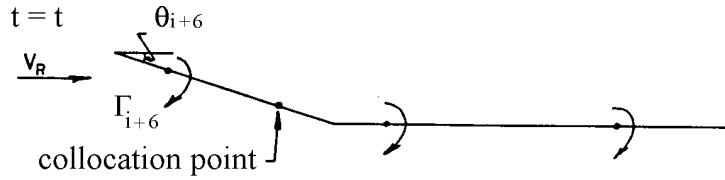


Fig. 10 (iv) - Unsteady reattachment, $\theta_{i+7} < 0.21$ rad.

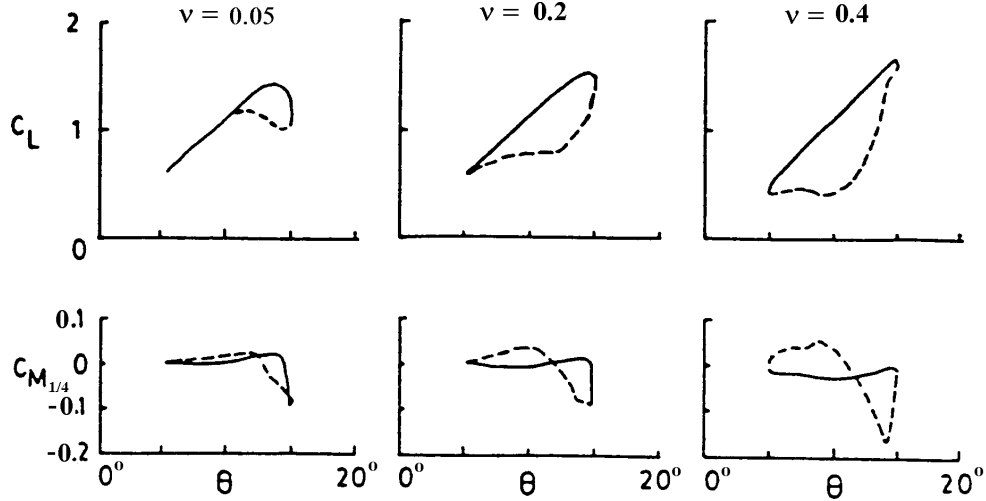


Fig 11 (i) – The effect of reduced frequency ν on the NACA 0012 aerofoil at $M_\infty = 0.3$ and $\theta = 10^\circ + 5^\circ \sin \omega t$ (experimental results)

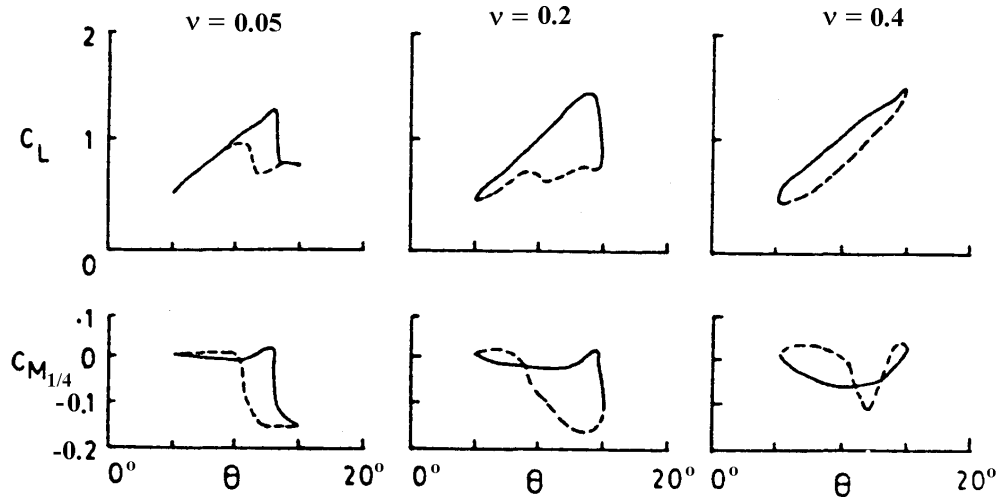


Fig 11 (ii) – The effect of reduced frequency ν on flat plate at $M_\infty = 0.3$ and $\theta = 10^\circ + 5^\circ \sin \omega t$ (axiomatic aerodynamic results)

3 . CONCLUSIONS

An axiomatic aerodynamic model has been developed for the general motion of a two-dimensional airfoil as it passes in and out of stall. Then the model has been applied to a dynamic stall situation with an oscillatory airfoil and compared with experimental results (Fig. 11(I, II)) [2]. Although the present axiomatic model does not represent the detailed conditions of the reattachment process in all considered motions ($\gamma = 0.05; 0.2; 0.4$) it is thought that the model gives realistic unsteady loads as compared to experimental values.

REFERENCES

1. Mc. Croskey, W.J., Carr L. W., McAlister K. W., Dynamic stall experiments on oscillating airfoils, AIAA Journal, 14 (1), 1976.
2. Mc. Croskey, W.J., The phenomenon of dynamic stall, NASA TM-81264, March, 1981.
3. Kawashiwa S, Yamasaki M., Aerodynamic response for the airfoil experiencing sudden change on angle of attack, Transactions of the Japan Society of Aeronautical and Space Sciences, 21(52), 1978.